International Journal of Fluid Mechanics Research, 47(4):291–307 (2020)

NUMERICAL PREDICTION OF FLOW THROUGH A P4119 PROPELLER USING A HYBRID MESH TECHNIQUE

N. Prakash,[1,*] D.G. Roychowdhury,[2] A. Muthuvel,[3] A.E. Kabeel,[4] Prasad Chandran,[1] Ali J. Chamkha,[5,6] & Ravishankar Sathyamurthy[1,4]

[1]*Department of Automobile Engineering, Hindustan Institute of Technology and Science, Chennai, India*

[2]*Hindustan Institute of Technology and Science, Chennai, India*

[3]*Department of Mechanical Engineering, Sai Ram College of Engineering, Hosur, India*

[4]*Mechanical Power Engineering Department, Faculty of Engineering, Tanta University, Egypt*

[5]*Mechanical Engineering Department, Prince Sultan Endowment for Energy and Environment, Prince Mohammad Bin Fahd University, Al-Khobar 31952, Saudi Arabia*

[6]*RAK Research and Innovation Center, American University of Ras Al Khaimah, P.O. Box 10021, Ras Al Khaimah, United Arab Emirates*

*Address all correspondence to: N. Prakash, Assoc. Professor, Department of Automobile Engineering, Hindustan Institute of Technology and Science, Chennai, India, E-mail: nprakrao1@gmail.com

Original Manuscript Submitted: 10/16/2018; Final Draft Received: 5/29/2020

A three-dimensional steady-state analysis of a three-bladed DTMB P4119 propeller is carried out with a hybrid mesh using the k–ε V2F turbulence model, and assuming the flow past the propeller to be laminar. The simulation is carried out for various advance ratios: $J = 0.5$, 0.833, 0.889, and 1.1. The predicted hydrodynamic coefficients, such as the thrust coefficient (K_t), torque coefficient (K_q), and coefficient of pressure (C_p), compare very well with experimental results for both the design as well as off-design advance ratios. Also, for the design advance ratio, both models predict the circumferentially averaged axial, radial, and tangential velocities very well. It is observed that the majority of the flow over the blade surface is laminar, and both the k–ε V2F and laminar models can capture the tip vortex very well. Hence, both models can be used to predict the hydrodynamic parameters effectively.

KEY WORDS: *CFD, propeller, hydrodynamic coefficients, moving reference frame, interface, turbulent, laminar, tip vortex*

1. INTRODUCTION

A marine propeller possesses a very intricate geometry, consisting of variable section profiles, chord lengths, and pitch angles. These features make the determination of the flow over a propeller an extremely challenging problem. Various techniques are used for the analysis of flow through marine propellers, including experimental methods, inviscid methods (panel methods), and viscous methods with the use of a Reynolds-averaged Navier–Stokes equation (RANSE) solver (Bogdan et al., 1998); and the global and local parameters, such as pressure and velocities, are measured. However, it is time-consuming and costly to carry out parametric studies. In an inviscid panel method (Brizzolara and Gaggero, 2008), the hydrodynamic parameters can be well predicted for a design advance ratio. However, the predictions are not as accurate in the case of off-design advance ratios. This may be due to neglect of the viscous effects. To overcome the limitations in the experimental and panel methods, the RANSE solver technique

NOMENCLATURE

c	blade section chord length, m
C_1	chord length at $0.7R$
C_p	coefficient of pressure, $C_p = \dfrac{P - P_0}{1/2\,\rho V_{\text{res}}^2}$
D	propeller diameter, m
R	propeller radius, m
F	maximum blade section camber, m
F/c	blade section camber–to–chord length ratio
f	local section camber,
f/F	chord-wise camber distribution
J	advance ratio, $J = \dfrac{V_{\text{in}}}{nD}$
K_t	thrust coefficient, $K_t = \dfrac{T}{\rho\, n^2 D^4}$
K_q	torque coefficient, $K_q = \dfrac{Q}{\rho\, n^2 D^5}$
n	speed of blade rotation, rps
P	pressure over the blade surface, N/m^2
p	pitch of propeller, m
P/D	pitch-to-diameter ratio
P_0	initial pressure, N/m^2
ρ	density of water, kg/m^3
Q	average torque of three blades, N-m
Re	Reynolds number, $\text{Re} = \rho\, V_{\text{in}} \dfrac{D}{\mu}$
Re_b	blade Reynolds number, $\text{Re}_b = \left[V_{\text{res}}^2 + (2\,\pi r n)^2\right]^{0.5} \dfrac{C_1}{\nu}$
r	local radius of the blade cross section, m
T	average thrust of three blades, N
$t_{\max}$	maximum blade section thickness, m
t	local section thickness, m
t/T	chord-wise thickness distribution
V_{in}	inlet velocity, m/s
V_r	radial velocity, m/s
V_{r1}	circumferentially averaged radial velocity, $V_{r1} = \dfrac{V_r}{V_{\text{in}}}$
V_{res}	resultant velocity, $V_{\text{res}} = V_{\text{in}} \left[1 + \left(\dfrac{\pi r/R}{J}\right)^2\right]^{0.5}$, m/s
V_t	tangential velocity, m/s
V_{t1}	circumferentially averaged tangential velocity, $V_{t1} = \dfrac{V_t}{V_{\text{in}}}$
V_z	axial velocity, m/s
V_{z1}	circumferentially averaged axial velocity, $V_{z1} = \dfrac{V_z}{V_{\text{in}}} - 1$
x/c	fraction of chord length
$\boldsymbol{\Phi}$	pitch angle, degree
ν	kinematic viscosity, $\nu = \dfrac{\mu}{\rho}$, m^2/s
μ	dynamic viscosity, Ns/m^2

(Brizzolara and Gaggero, 2008; Streckwall, 1998; Bong, 1998; Shotaro, 1998; Chen and Stern, 1998; Sánchez, 1998; Kyung et al., 1998; Xiao and Walters, 2012) is being universally used by many researchers. Brizzolara and Gaggero (2008) carried out an extensive study using a panel method and a RANSE method, and concluded that for low advance ratios and for off-design conditions, a RANSE solver predicts better. Streckwall (1998) carried out an analysis of flow through the marine propeller P4119 with the standard k–ε turbulence model. However, he suggested the need to carry out the grid independence for better accuracy. Bong (1998) used a finite volume technique using unstructured meshes along with the standard k–ε turbulence model (Launder and Spalding, 1974) to analyze the P4119 propeller.

The thrust coefficient (K_t) predicted for the design condition matched well with the experimental results (Jessup, 1989), but the torque coefficient (K_q) was overpredicted by 10% compared to the measured data. However, they failed to capture the wake behind the propeller, and suggested carrying out the analysis with other turbulence models for better prediction. Shotaro (1998) carried out numerical simulations around a marine propeller with RANSE. The modified Baldwin–Lomax zero-equation turbulence model was adopted for turbulent closure. The equations were discretized by the cell-centered, finite volume method with the third-order upwind scheme. The predictions of thrust

and torque coefficients were about 10% higher than the experimental data for the design advance ratio. Based on the study, the author suggested carrying out the analysis with a better grid resolution. Chen and Stern (1998) carried out an unsteady three-dimensional analysis of P4119 at design conditions using the Baldwin–Lomax turbulence model. The thrust and torque coefficients were underpredicted by 4% and 0.7%, respectively. The authors suggested a better mesh refinement to capture the tip vortex, boundary layer, and blade wake behavior. Sánchez (1998) carried out a performance analysis for the P4119 propeller, using the FINFLO finite volume code, in a rotating coordinate system using the k-ε turbulence model. The predictions of K_t and K_q for the propeller were within 1.5% of experimental values for advance coefficients close to the design value. Although the flow patterns were generally well predicted, the author suggested the use of more sophisticated turbulence models for better prediction of tip vortex flow. Kyung et al. (1998) carried out an analysis around the P4119 propeller, using an H-type grid with the two-layer k–ε turbulence model. His results predicted the existence of two different zones—laminar and turbulent—over the blade surface. He also suggested the use of a block mesh to capture the tip vortex. Xiao et al. (2012) carried out simulations using both fully turbulent and transition-sensitive eddy viscosity turbulence models for the P5168 five-bladed propeller, and predicted the existence of a laminar region up to 40% of the blade surface. Prakash et al. (2014) carried out both steady and unsteady analyses for the simulation of the P4119 propeller with SST Menter k–ω, Standard k–ω, k–ε AKN, and k–ε V2F turbulence models for the design advance coefficient, using a polyhedral mesh. The predicted results were within 5% for K_t and 6% for K_q (Jessup, 1989). They also concluded that of the four turbulence models, the k–ε V2F model predicts best in comparison with the experimental data (Jessup, 1989). The authors also suggested adopting a structured/prism mesh for further improvement.

Based on the literature survey, it was observed that although the hydrodynamic coefficients (K_t and K_q) were well predicted for the design advance ratio, predictions for the off-design value need to be improved. Almost all the researchers failed to capture the tip vortex flow, and suggested the use of a better grid and turbulence model. It is also suggested to use a transition model (Kyung et al., 1998; Xiao et al., 2012), as the flow along the propeller consists of both laminar and turbulent regimes.

Hence, a study has been carried out for the P4119 propeller, with a hybrid mesh technique consisting of a prism layer mesh along with a polyhedral mesh, for both design and off-design advance coefficients $J = 0.833$, 0.5, 0.889, and 1.1. For the analysis, the k–ε V2F model and the laminar model are used for comparison. The results obtained from the above analysis are presented here.

2. NUMERICAL APPROACH

The computational resources (both hardware and software) for the present study are shown in Appendix A.

2.1 Governing Equations

2.1.1 Generalized Governing Equations

Continuity equation:

$$\frac{\partial(\rho u)}{\partial x} + \frac{\partial(\rho v)}{\partial y} + \frac{\partial(\rho w)}{\partial z} = 0 \tag{1}$$

Momentum equation:

$$\frac{\partial}{\partial t}(\rho u_i) + \frac{\partial}{\partial x_j}(\rho u_i u_j) = -\frac{\partial p}{\partial x_i} + \frac{\partial \tau_{ij}}{\partial x_j} + \frac{\partial}{\partial x_j}(-\overline{\rho u_i' u_j'}) + f_i \tag{2}$$

where

$$\tau_{ij} = \mu\left(\frac{\partial u_i}{\partial x_j} + \frac{\partial u_j}{\partial x_i}\right) \tag{3}$$

and $-\overline{\rho u_i' u_j'}$, which is known as Reynolds stress, gives rise to a closure problem, as the values are unknown. Normally $u_i' u_j'$ is related to the mean velocities by the eddy viscosity concept, which is given by

$$-\overline{\rho u_i' u_j'} = \mu_t \left(\frac{\partial u_i}{\partial x_j} + \frac{\partial u_j}{\partial x_i} \right) - \frac{2}{3} \rho k \delta_{ij} \tag{4}$$

where μ_t is the turbulent viscosity and k is the turbulent kinetic energy.

2.1.2 Generalized Governing Equations for V2F Turbulence Model

The turbulent viscosity is defined as

$$\mu_t = \rho \, C_\mu \overline{\upsilon^2} \, T \tag{5}$$

and the turbulent quantities in addition to standard k and ε are obtained from two more equations, the transport equation for $\overline{\upsilon^2}$:

$$\frac{\partial \rho \overline{\upsilon^2}}{\partial t} + \frac{\partial}{\partial x_j} \left(\rho u_j \overline{\upsilon^2} \right) = \rho k f - \rho \frac{\overline{\upsilon^2}}{k} \varepsilon + \frac{\partial}{\partial x_j} \left[\left(\mu + \frac{\mu_t}{\sigma_{\overline{\upsilon^2}}} \right) \frac{\partial \overline{\upsilon^2}}{\partial x_j} \right] \tag{6}$$

and the elliptic equation for relaxation function f:

$$L^2 \nabla^2 f - f = \frac{C_1 - 1}{T} \left(\frac{\overline{\upsilon^2}}{k} - \frac{2}{3} \right) - C_2 \frac{P_k}{\varepsilon} \tag{7}$$

where the turbulence length scale L is

$$L = C_L \max \left[\frac{k^{3/2}}{\varepsilon}, C_\eta \left(\frac{\upsilon^3}{\varepsilon} \right)^{1/4} \right] \tag{8}$$

and the turbulent time scale T is

$$T = \max \left[\frac{k}{\varepsilon}, C_T \left(\frac{\upsilon}{\varepsilon} \right)^{1/2} \right] \tag{9}$$

They are bounded with their respective Kolmogorov definition (reliability constraints can also be applied as below).

The coefficient used is

$$C_\mu = 0.22, \quad \sigma_{\overline{\upsilon^2}} = 1, \quad C_1 = 1.4, \quad C_2 = 0.45, \quad C_T = 6, \quad C_L = 0.25, \quad \text{and } C_\eta = \quad 85$$

2.2 Model Geometry and Grid Generation

The David Taylor Model Basin (DTMB) P4119 (Jessup, 1989) propeller model has been considered for the study. It is a right-handed three-bladed propeller with no skew and a simple geometry, with a diameter of $D = 0.305$ m, as shown in Table 1. For developing the blade profile, an aerofoil profile of NACA66 is selected (Jessup, 1989). The blades are developed in such a way that the aerofoil sections are arranged one above the other and splined to generate a blade profile. The blades are then simply mounted on a cylinder, which serves as the shaft. Before the shaft, a hub is provided for free flow to the propeller blades. The model thus created in SOLIDWORKS is shown in Fig. 1(a), and then imported to STAR-CCM+ for meshing and analysis. Figure 1(b) shows the general definition of an aerofoil. The computational domain has been created with a cylinder surrounding the propeller and aligned to the hub axis. Figure 2 shows a schematic diagram of the computational domain, whose diameter and length are 7.3 and 13.7 times the propeller diameter (Robert, 1971), respectively. All three blades are used for computation. The computational domain is subdivided into two—a moving and a stationary region. The stationary region is attached to the computational domain, and the moving region is with the propeller. To facilitate smooth data transfer between the stationary and the rotating region, a suitable interface with 1.5 times the propeller diameter (Robert, 1971) is introduced between the regions. There is no physical separation in space between the two boundaries comprising the interface. Appropriate governing equations are solved in each fluid zone. Single reference frame equations are used in the rotating zones.

TABLE 1: Geometrical data (based on the results of Sánchez, 1998)

S. No	r/R	c/D	P/D	t_{max}/c	F/c
1	0.30	0.285550	1.0000	0.15530	0.02318
2	0.40	0.318870	1.0000	0.11800	0.02303
3	0.50	0.345968	1.0000	0.09160	0.02182
4	0.60	0.363141	1.0000	0.06960	0.02072
5	0.70	0.364086	1.0000	0.05418	0.02003
6	0.80	0.342423	1.0000	0.04206	0.02003
7	0.90	0.284605	1.0000	0.03321	0.01817
8	0.95	0.218593	1.0000	0.03228	0.01631
9	1.00	0.126036	1.0000	0.03160	0.01175

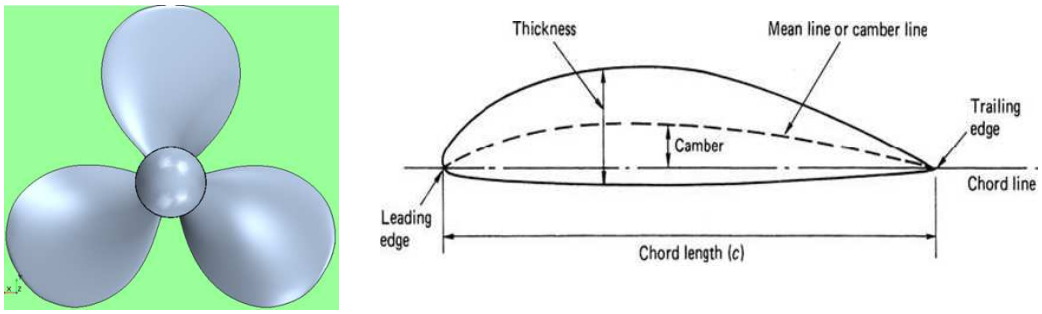

(a) (b)

FIG. 1: (a) Propeller model, (b) general definition of an aerofoil section

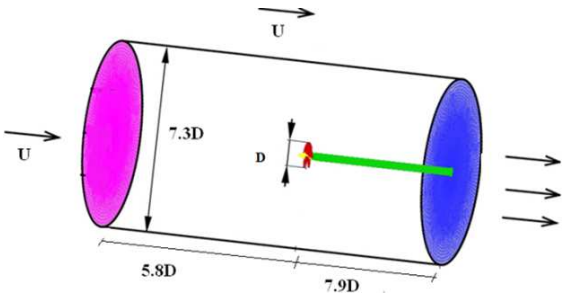

FIG. 2: Computational domain

A hybrid mesh consisting of prismatic mesh and polyhedral mesh is generated. First, a prismatic mesh is generated for the propeller, with 25 layers near the propeller surface, with a stretch factor of 1.1, as shown in Fig. 3, after which the polyhedral mesh is generated for the domain, hub, and interface. The prism layer mesh is used for better capturing the boundary layer over the propeller blades. The y+ value is maintained based on the requirement of the turbulence models used for the computations. Figure 4 shows the grid independence study for hybrid mesh.

2.3 Boundary Conditions

Appropriate boundary conditions are specified to simulate the open water tunnel test carried out by Robert (1971). At the inlet, a uniform velocity profile is specified, while on the exit, boundary pressure is specified. On the lateral boundary, a free-stream boundary condition is imposed. A no-slip condition is imposed on the blade and hub surfaces.

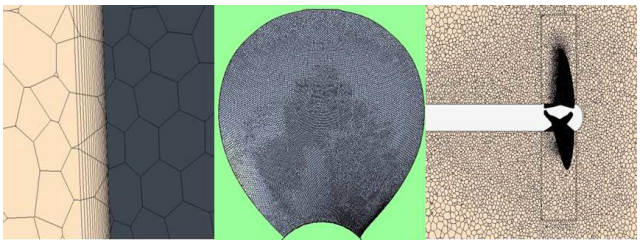

FIG. 3: Grid generation

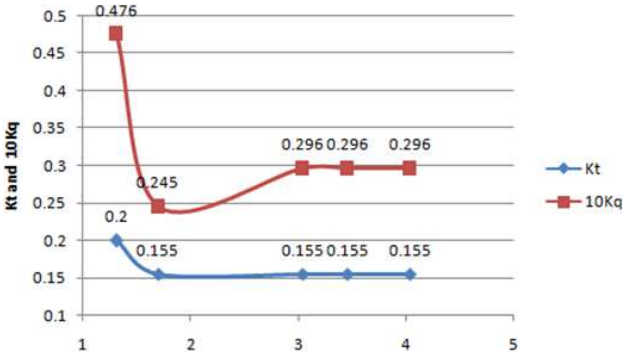

FIG. 4: Grid independence study for hybrid mesh

The material property for water is specified. The inlet parameters for various advanced coefficients are shown in Table 2. The values of turbulent kinetic energy (k), dissipation rate (ω), and specific dissipation rate (ε) at the inlet are calculated as follows:

$$k = u^2 \times 10^{-4}, \text{ J/kg, which corresponds to a turbulence intensity of } \sim 0.86\%.$$

$$\omega = \frac{\rho k}{100\mu}, /s, \quad \varepsilon = \omega k, \text{ J/kg-s}$$

2.4 Methodology

Three-dimensional numerical analysis of the flow through the P4119 propeller is carried out with the general-purpose RANSE solver STAR-CCM+. The analysis is carried out with the k–ε V2F turbulence model, as it is observed to predict better than other turbulence models (Prakash et al., 2014) and the laminar model. During the analysis, the maximum residuals from continuity, x-momentum, y-momentum, z-momentum, and turbulence are restricted to

TABLE 2: Various advance ratios (J)

S. No.	Advance ratio J	Velocity V (m/s)	Reynolds number $Re \times 10^6$	Blade Reynolds number $Re_b \times 10^6$	Turbulent kinetic energy $k \times 10^{-4}$ (J/kg)	Turbulent dissipation rate ω (/sec)	Specific dissipation rate $\varepsilon \times 10^{-4}$ (J/kg-s)	Speed n (rps)
1	0.5	1.525	0.59	1.374	2.3256	2.9946	6.964	10
2	0.833	2.4	1	1.404	6.4516	8.3350	53.774	
3	0.889	2.711	1.06	1.411	7.3490	9.4630	69.54	
4	1.1	3.355	1.32	1.439	11.256	14.494	163	

10^{-6} as convergence criteria. Initially, 300 iterations are carried out with the first-order upwind scheme. Then the second-order upwind scheme is used for further iterations until convergence is achieved. Numerical simulation is carried out for the design advance coefficient of $J = 0.833$ and off-design conditions $J = 0.5$, 0.889, and 1.1 by changing the velocity, as shown in Table 2. The grid independence study was carried out using the SST Mentor k–ω turbulence model as shown in Table 3.

Table 4 shows the thrust and torque coefficients obtained for various turbulence models and compared with the experimental results. It is observed that for thrust coefficient the values are within 2% to 9.58% compared to experimental values. k–ε V2F model overpredicts by 2% whereas it is 8.90% for the laminar model. All the models predict the torque coefficient within 1.43% to 6.43%. Here, the laminar model predicts within 1.43% whereas the k–ε AKN model predicts within 3.21% from the experimental values. The k–ε V2F model predicts within 3.93%, which is very near the value predicted by the k–ε AKN model. Thus for further analysis k–ε V2F and laminar models are used.

Also, in order to verify whether the k–ε V2F model is showing better results with only the 3.46 million mesh cells or also with other cells, the results below are also captured and verified. The average cell size is 0.00055 mm. The refinement of the mesh was done in order to achieve fine mesh near the edges of the propeller blade and also near the wall boundary.

Thrust and torque coefficients for designed advance coefficients for $J = 0.833$ by using the k–ε V2F model for all mesh is shown in Table 5, with 1.31, 1.7, 3.04, 3.46, and 4.04 million cells. The analysis was carried out for 1500 iterations, for a duration of approximately 96 hr, by running the simulation continuously.

3. RESULTS AND DISCUSSION

3.1 Design Advance Coefficient ($J = 0.833$)

The hydrodynamic coefficients K_t and K_q are calculated from $K_t = T/(\rho\, n^2 D^4)$ and $K_q = Q/(\rho\, n^2 D^5)$, where T is the average thrust for the three blades and Q is the average torque for the three blades.

TABLE 3: Thrust and torque coefficients for designed advance coefficient to attain grid sensitivity for DTMB P4119 for hybrid mesh

Grid (million)	Turbulence models	Thrust coefficient (K_t)	Difference	Torque coefficient ($10K_q$)	Difference
		Analysis		Analysis	
1.31	SST Mentor k–ω	0.200	—	0.476	—
1.7		0.155	0.045	0.245	0.231
3.04		0.155	0	0.296	0
3.46		0.155	0	0.296	0
4.04		0.153	0.002	0.296	0

TABLE 4: Comparison of thrust and torque coefficients for grid sensitive cell for DTMB P4119 (hybrid mesh)

Turbulence models	Thrust coefficient (K_t)		% Deviation	Torque coefficient ($10K_q$)		% Deviation
	Exp[6]	Analysis		Exp[6]	Analysis	
k–ε AKN	0.146	0.160	9.58	0.28	0.289	3.21
k–ε V2F		0.149	2.00		0.291	3.93
Standard k–ω		0.155	6.16		0.298	6.43
SST Mentor k–ω		0.155	6.16		0.296	5.71
Laminar		0.159	8.90		0.284	1.43

TABLE 5: Thrust and torque coefficients for designed advance coefficient for $J = 0.833$ by using k–ε V2F model for all mesh

Grid (million)	Turbulence models	Thrust coefficient (K_t)		% Deviation	Torque coefficient ($10K_q$)		% Deviation
		Exp (Jessup, 1989)	Analysis		Exp (Jessup, 1989)	Analysis	
1.31	k–ε V2F	0.146	0.200	+27.11	0.280	0.476	+41.17
1.7			0.155	+5.81		0.245	–12.5
3.04			0.153	+5.81		0.296	+5.40
3.6			0.149	+2		0.291	+3.78
4.04			0.152	+3.95		0.295	+5.08

Table 6 shows the thrust and torque coefficients obtained for the k–ε V2F turbulence model and the laminar model, and compared with the experimental results (Jessup, 1989). It is observed that for the thrust coefficient, the k–ε V2F model overpredicts by 2%, whereas it is 8.17% for the laminar case. However, for the torque coefficient, the V2F model overpredicts by 3.78%, whereas the laminar case predicts within 1.41% of the experimental values.

The variation of the coefficient of pressure for $J = 0.833$ along the chord length at radius $0.7R$ and $0.9R$, for both the pressure and suction sides of the propeller blade, are compared with the experimental data as shown in Fig. 5. It can be seen that both models predict C_p values very well for $0.7R$. For $0.9R$, there is a slight deviation at the leading edge for the suction side, and at the trailing edge for the pressure side. As this section is very near the tip of the blade, flow through this section may be influenced by tip vortex flow, leading to the deviation.

Figure 6 shows the variation of the circumferentially averaged axial and radial velocity at $z/R = –0.3$ for $J = 0.833$, with various r/R, from root to tip of the propeller blade. It is observed that the axial velocity predicted by both the k–ε V2F and the laminar models agrees very well with the experimental data (Kyung et al., 1998), with maximum deviations from $r/R = 0.3$ to 0.4. This may be due to the presence of the hub, which leads to unsatisfactory development of the boundary layer. The radial velocity also matches well with the experimental data, except from $r/R = 0.3$ to 0.5, for similar reasons.

Figure 7 shows the variation of the circumferentially averaged axial, radial velocity, and tangential velocity at $z/R = 0.3281$ for k–ε V2F and laminar model for $J = 0.833$. It can be seen that both models predict radial and tangential velocities very well with respect to the experimental data (Kyung et al., 1998). However, for axial velocity, there is a large deviation near $r/R = 0.3$. This may be due to the presence of the hub, which influences the flow development past the propeller. As expected, the deviation is greater for the k–ε V2F than for the laminar model.

Figure 8 shows the wall shear stress distribution over the blade surface for both the k–ε V2F and the laminar models, in the vertical direction from near the hub to the blade tip, for both the suction side and the pressure side, at the design advance coefficient, $J = 0.833$. For the suction side, the wall shear stress predicted by the k–ε V2F model increases gradually from the hub to $x/c = 0.45$, after which the gradient increases sharply, indicating the transition from the laminar to the turbulent region. For the laminar model, a gradual increase in wall shear stress is observed

TABLE 6: Thrust and torque coefficients for designed advance coefficient for $J = 0.833$

Grid (million)	Turbulence models	Thrust coefficient (K_t)		% Deviation	Torque coefficient ($10K_q$)		% Deviation
		Exp (Jessup, 1989)	Analysis		Exp (Jessup, 1989)	Analysis	
3.46	k–ε V2F	0.146	0.149	2	0.280	0.291	3.78
	Laminar		0.159	8.17		0.284	1.41

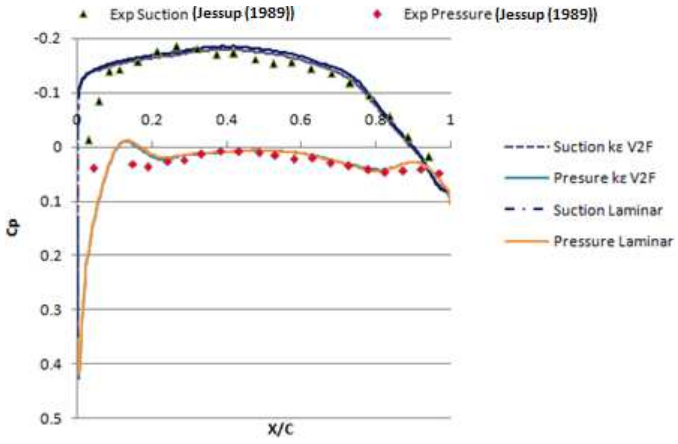

(a) $0.7R$

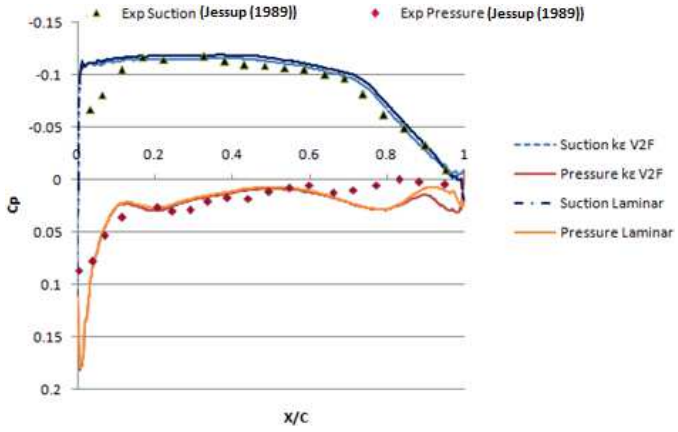

(b) $0.9R$

FIG. 5: Variation of coefficient of pressure along the chord length for $J = 0.833$

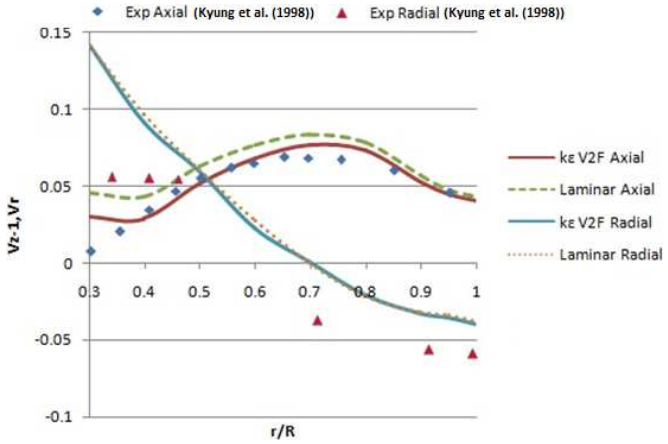

FIG. 6: Circumferentially averaged axial and radial velocity at $z/R = –0.3$ for k–ε V2F and laminar for $J = 0.833$

until $x/c = 0.95$, after which a there is a sudden increase in wall shear stress. This indicates the existence of a laminar region on the suction side of the blade up to 45% predicted by the k–ε V2F model, and up to 95% by the laminar

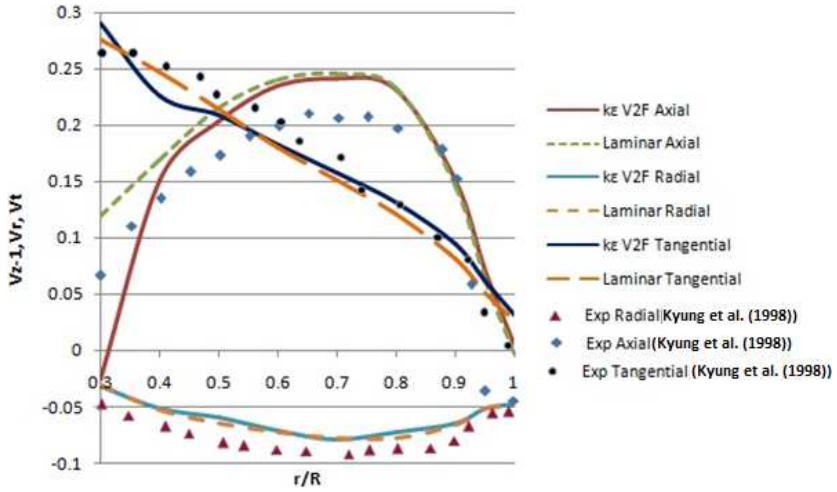

FIG. 7: Circumferentially averaged axial, radial, and tangential velocity at $z/R = 0.3281$ for k–ε V2F and laminar for $J = 0.833$

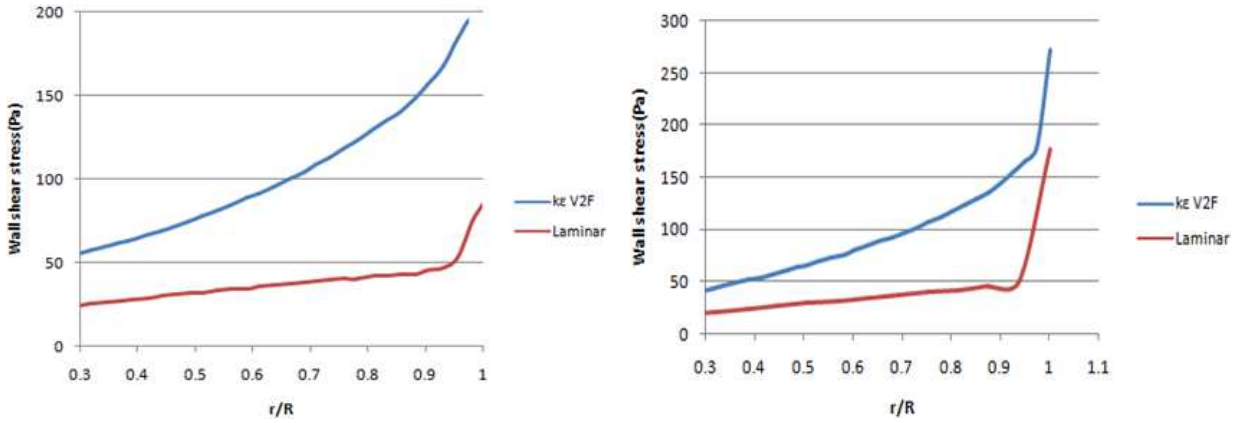

(a) Suction side (b) Pressure side

FIG. 8: Wall shear stress distribution over the blade surface for $J = 0.833$ in the vertical direction

model. For the pressure side, the wall shear stress predicted by both the models shows similar trends as observed for the suction side. For the k–ε V2F model, the laminar-to-turbulent transition starts from $x/c = 0.65$.

Figures 9 and 10 show the skin friction distribution for the k–ε V2F and laminar models on both the suction and pressure sides, which supports the above explanation for the existence of a laminar region over the blade surface (Fig. 9). The contour predicted by the laminar model shows that the majority of flow is laminar for both the suction and pressure sides, whereas it is different for the suction and pressure sides as predicted by the k–ε V2F model.

Figure 11 shows the formation of free vortices by the blade surface from upstream of the propeller to downstream of the propeller blade for both the k–ε V2F and laminar models. The vortices are taken at locations from upstream to downstream at $z/R = $ –0.1312, 0.0, 0.0656, 0.1969, 0.2625, and 0.3281, respectively. It can be seen that no vortices are formed upstream of the propeller blade. But the vorticity starts forming at $z/R = 0.0$ and grows toward the downstream of the propeller blade, which finally leads to the formation of blade wake.

3.2 Off-Design Advance Coefficient ($J = 0.5$, 0.889, and 1.1)

Analysis is carried out for off-design advance ratios 0.5, 0.889, and 1.1. Special attention is given to $J = 0.5$, as it indicates a higher loading condition. This is important because of increased discrepancies observed between the

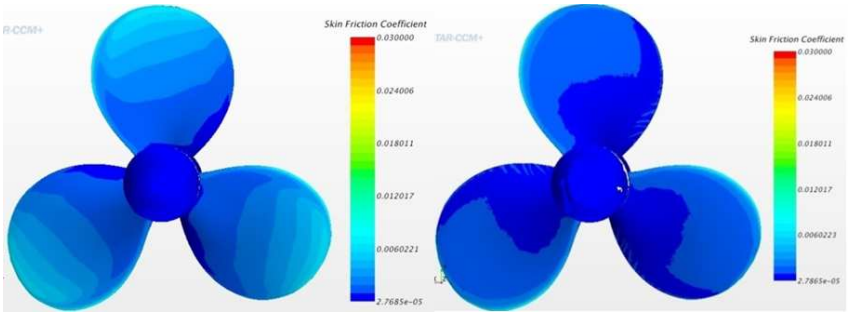

(a) k–ε V2F (b) Laminar

FIG. 9: Skin friction distribution on the suction side for $J = 0.833$

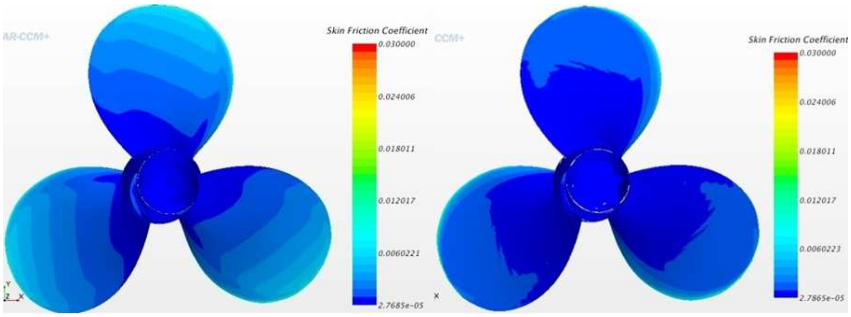

(a) k–ε V2F (b) Laminar

FIG. 10: Skin friction distribution on the pressure side for $J = 0.833$

predicted results and the experimental data using a fully turbulent RANSE simulation (Ito, 1987; Uto, 1992, 1993, 1994). At higher loading conditions, the blade Reynolds number is lower, and the assumption of the existence of fully turbulent conditions may not be correct. Table 7 shows the thrust and torque coefficients obtained for these advance coefficients. It is observed that the k–ε V2F model overpredicts the thrust coefficient by 7.16% for $J = 0.5$, 0.76% for $J = 0.889$, and 19.48% for $J = 1.1$, whereas for the laminar model, these values are 7.76%, 3.7%, and 28.63%, respectively, for the corresponding advance ratios. For the torque coefficient, the maximum deviation predicted by the k–ε V2F model is 8.69% for $J = 1.1$. For $J = 0.5$ and 1.1, the laminar model predicts better than the k–ε V2F model when compared with the experimental data (Jessup, 1989). This shows that both models predict the torque coefficients very well, but the prediction of the thrust coefficient for $J = 1.1$ is not as good for both models.

The variation of the coefficient of pressure along the chord length for $J = 0.5$ and 1.1 at the $0.7R$ section on the suction and pressure sides of the propeller blade is shown in Figs. 12 and 13, respectively, along with the experimental data (Haimov et al., 2007). It can be seen that, in general, for both models, the predicted values match very well with the experimental data (Haimov et al., 2007) for $J = 0.5$, except for the leading edge, where the maximum deviation is 15%. For $J = 1.1$, the predicted values match very well with the experimental data for the suction side. However, there is a deviation between the predicted and experimental data at the pressure side, at both the leading and trailing edges, with a maximum deviation of 12%. Clustering more grids near the leading and trailing edges may lead to better capture of the boundary layer development, thereby reducing the deviations.

Figure 14 shows the wall shear stress distribution over the blade surface for both the k–ε V2F and laminar models, in the vertical direction, from near the hub to the blade tip, on the suction side, for $J = 0.5$. For the k–ε V2F model, the suction side indicates that the laminar region covers 45% of the blade surface, after which it is turbulent. For the laminar model, the shear stress varies gradually up to 70% of the blade surface, after which there is a sudden increase in the shear stress gradient. For the pressure side, the shear stress predicted by the k–ε V2F model varies gradually up to 48% of the blade surface, after which there is a sudden increase in the shear stress gradient. It shows that the

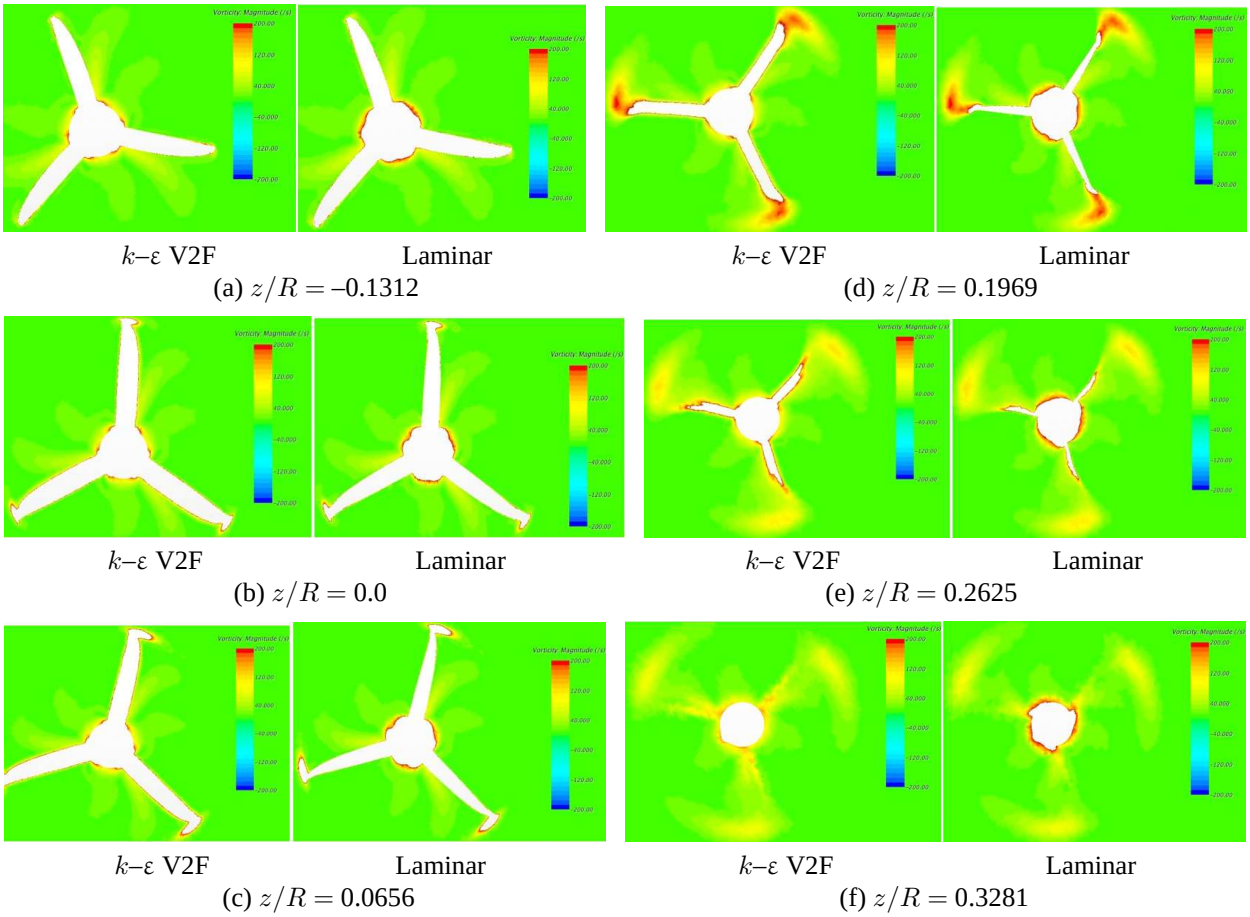

FIG. 11: Formation of free vortices for k–ε V2F and laminar model for $J = 0.833$

TABLE 7: Thrust and torque coefficients for off-design advance coefficients

Grid (million)	Turbulence models	Thrust coefficient (K_t)		% Deviation	Torque coefficient ($10K_q$)		% Deviation
		Exp (Haimov et al., 2007)	Analysis		Exp (Haimov et al., 2007)	Analysis	
3.46				$J = 0.5$			
	k–ε V2F	0.285	0.307	7.16	0.479	0.509	5.89
	Laminar		0.309	7.76		0.498	3.81
				$J = 0.889$			
	k–ε V2F	0.130	0.131	0.76	0.266	0.259	2.63
	Laminar		0.135	3.70		0.247	7.14
				$J = 1.1$			
	k–ε V2F	0.0314	0.039	19.48	0.105	0.115	8.69
	Laminar		0.044	28.6		0.104	0.95

laminar region extends to 66% of the blade surface for the pressure side predicted by the k–ε V2F model. With the laminar model, the laminar region extends to 92% of the blade surface, as on the suction side of the blade.

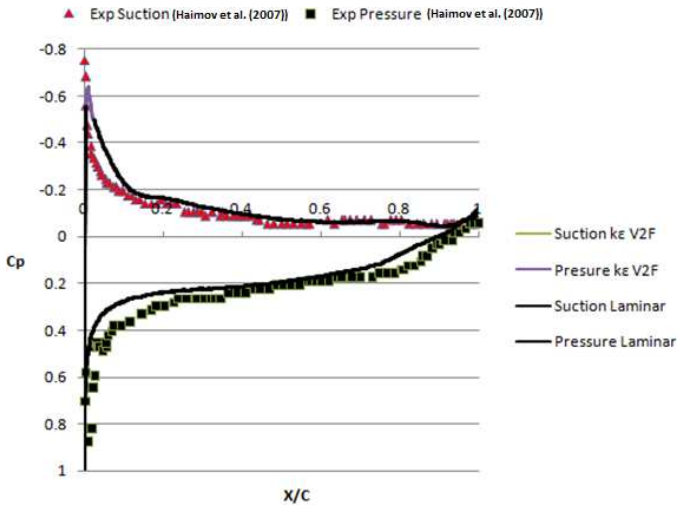

FIG. 12: Variation of coefficient of pressure along the chord length at $r = 0.7R$ for $J = 0.5$

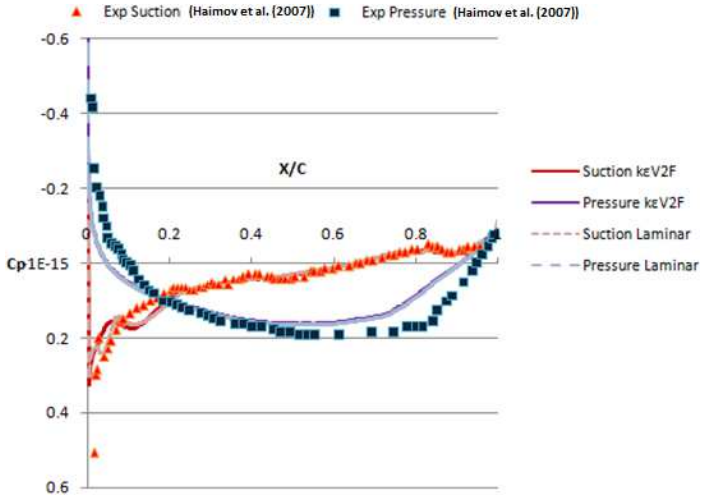

FIG. 13: Variation of coefficient of pressure along the chord length at $r = 0.7R$ for $J = 1.1$

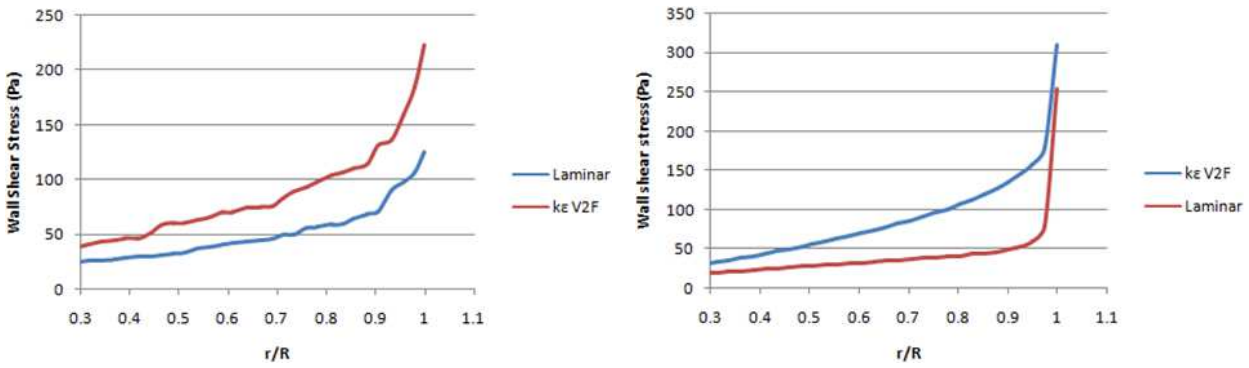

(a) Suction side (b) Pressure side

FIG. 14: Wall shear stress distribution over the blade surface for $J = 0.5$ in the vertical direction

Figures 15 and 16 show the contours on the suction and pressure sides of the blade for $J = 0.5$, which is in line with the argument made for Fig. 14. For the other advance ratios, $J = 0.889$ and 1.1, the shear stress distribution is shown in Figs. 17–20, which clearly demonstrate the existence of a laminar region over the blade surface on both the suction and pressure sides, as predicted by the laminar model.

4. CONCLUSION

Numerical simulation of flow through the marine propeller DTMB P4119 is carried out with a hybrid mesh consisting of prismatic and polyhedral meshes. The simulation is carried out with the k–ε V2F turbulence model and the laminar model, for advance ratios $J = 0.833$, 0.5, 0.889, and 1.1. It is observed that both models predict global as well as

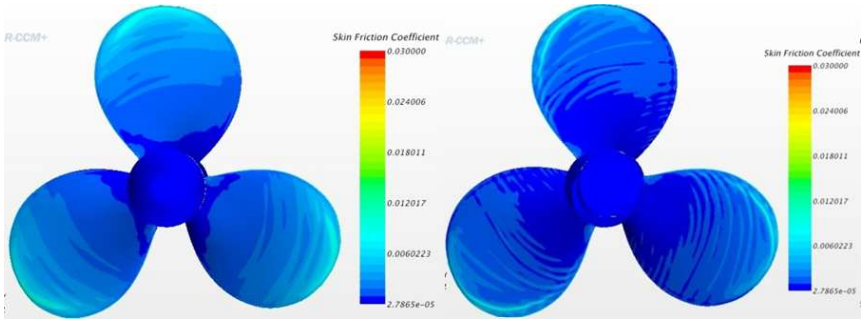

(a) k–ε V2F (b) Laminar

FIG. 15: Skin friction distribution on the suction side for $J = 0.5$

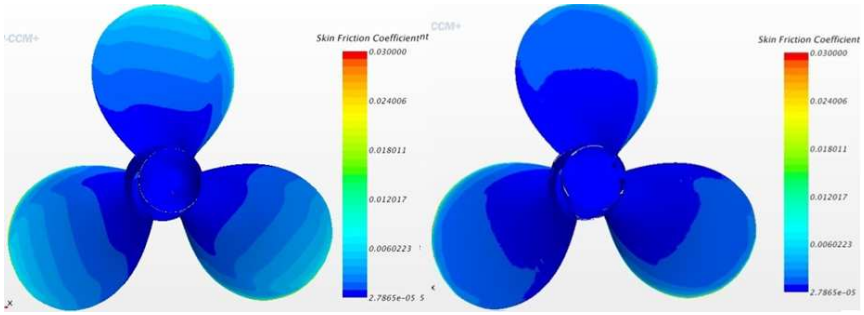

(a) k–ε V2F (b) Laminar

FIG. 16: Skin friction distribution on the pressure side for $J = 0.5$

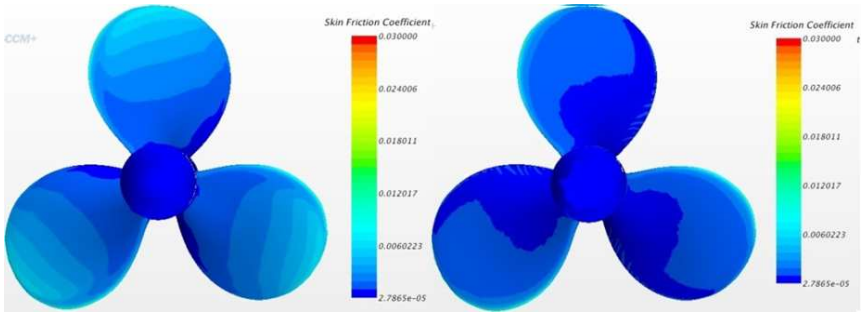

(a) k–ε V2F (b) Laminar

FIG. 17: Skin friction distribution on the suction side for $J = 0.889$

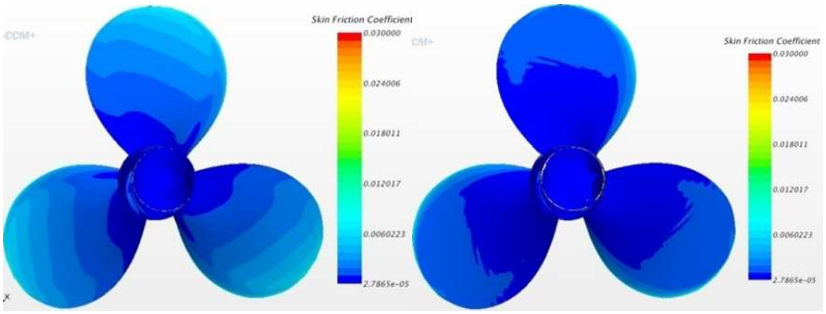

(a) k–ε V2F (b) Laminar

FIG. 18: Skin friction distribution on the pressure side for $J = 0.889$

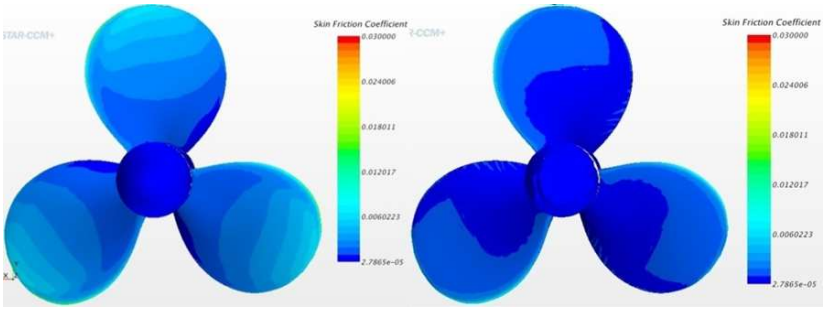

(a) k–ε V2F (b) Laminar

FIG. 19: Skin friction distribution on the suction side for $J = 1.1$

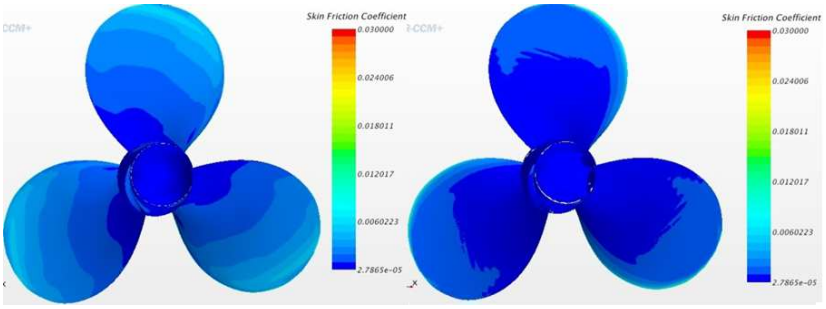

(a) k–ε V2F (b) Laminar

FIG. 20: Skin friction distribution on the pressure side for $J = 1.1$

local flow behavior well for the design advance ratio, $J = 0.833$. The hydrodynamic coefficients K_t and K_q are overpredicted by 2% and 3.7% with the k–ε V2F model, whereas with the laminar model the values are 8.17% and 1.41%, respectively. Both models predict the coefficient of pressure on the suction and pressure sides at $0.7R$ and $0.9R$ very well with respect to the experimental data. Deviations of 12.5% and 14.28% are observed for the circumferentially averaged axial velocity at $z/R = 0.3281$ for the k–ε V2F and laminar models, respectively, whereas both the k–ε V2F model and the laminar model predict radial velocity very well with respect to the experimental data. The tip vortex is also captured well by both the k–ε V2F and laminar models. The shear stress distribution is also predicted on the blade surface for both the k–ε V2F and laminar models on the suction and pressure side, respectively, for $J = 0.833$. The k–ε V2F model indicates that the laminar region covers 45% of the blade surface on the suction side, after which it is turbulent. For the pressure side, the shear stress predicted by the k–ε V2F model varies gradually up to 65% of the blade surface, after which there is a sudden increase in the shear stress gradient. This shows that

the laminar region extends up to 65% of the blade surface on the pressure side, as predicted by the k–ε V2F model. However, the laminar model predicts the laminar region to exist up to 95% of the blade surface for both the suction and pressure sides. This clearly establishes that the major portion of the flow over the blade surface is laminar. Also, both models predict the hydrodynamic parameters very well for off-design advance ratios, especially for $J = 0.5$. From the above study, it can be concluded that both the k–ε V2F and laminar models with hybrid mesh can be used for efficient prediction of the flow over the DTMB P4119 propeller, for either design or off-design advance ratios.

ACKNOWLEDGMENTS

This work is carried out under the Naval Research Board, Project No. NRB-135/HYD/07-08, titled “Numerical Simulation of Hull-Propeller Interaction for Underwater Vehicle with Mounted Propellers.” The authors express their heartfelt thanks to the NRB for providing the research grant.

REFERENCES

Bogdan, G., Danicla, G., and Davis, L., Steady and Unsteady Marine Propeller Hydrodynamic Calculation by Means of the Direct Boundary Element Method, *22nd ITTC Propuls. Committee; Propeller RANS/ Panel Method Workshop*, France, pp. 273–282, 1998.

Bong, J.C., Application of CFD to P4119 Propeller, *22nd ITTC Propeller RANS/Panel Method Workshop*, France, 1998.

Brizzolara, D.V.S. and Gaggero, S., A Systematic Comparison between RANS and Panel Methods for Propeller Analysis, *Proc. of 8th Int. Conf. on Hydrodynamics (ICHD’08)*, Nantes, France, 2008.

Chen, B. and Stern, F., RANS Simulation of Marine Propulsor P4119 at Design Condition, *22nd ITTC Propulsion Committee; Propeller RANS/ Panel Method Workshop*, France, 1998.

Haimov, E., Terceno, M., and Trejo, I., Use of Commercial Code for Open Water Propeller Characteristics, *Proc. of the 10th Numerical Towing Tank Symp.*, Hambergo, Alemania, Germany, 2007.

Ito, M., Calculation of Viscous Effects on Propeller Open Characteristics, *Trans. West-Japan Soc. Nav. Archit.*, vol. **73**, pp. 83–96, 1987.

Jessup, S., An Experimental Investigation of Viscous Effects of Propeller Blade Flow, PhD, The Catholic University of America, 1989.

Kyung, N.C., Stern, F., and Keh-Sik, M., Steady Viscous Flow Field around Propeller P4679, *22nd ITTC Propulsion Committee; Propeller RANS/ Panel Method Workshop*, France, 1998.

Prakash, N., Muthuvel, A., and Roychowdhury, D.G., Numerical Simulation of a Three Bladed Marine Propeller in Steady and Unsteady State, *Int. J. Appl. Mechan. Mater.*, vols. **592–594**, pp. 1136–1141, 2014.

Robert, J.B., Design Cavitation Performance and Open-Water Performance of a Series of Research Skewed Propellers, David W. Taylor Naval Ship Research and Development Center, Bethesda, MD, Rep. No. 3339, 1971.

Sánchez, C.A., DTRC Propeller 4119 Calculations at VTT, *22nd ITTC Propulsion Committee; Propeller RANS/ Panel Method Workshop*, France, 1998.

Shotaro, U.T.O., RANS Simulation of Turbulent Flow around DTMB4119 Propeller, *22nd ITTC Propulsion Committee; Propeller RANS/ Panel Method Workshop*, France, pp. 427–492, 1998.

Streckwall, H., Hydrodynamic Analysis of DTRC Propeller 4119 in Steady Flow Using a Commercial Navier–Stokes Solver, *22nd ITTC Propulsion Committee; Propeller RANS/ Panel Method Workshop*, France, 1998.

Uto, S., Basic Study on the Scale Effect of the Viscous Flow around a Marine Propeller, *J. Kansai Soc. Nav. Archit.*, vol. **222**, pp. 33–39, 1994.

Uto, S., Computation of Incompressible Viscous Flow around a Marine Propeller, *Jpn. Soc. Nav. Archit. Ocean Eng.*, vol. **172**, pp. 213–224, 1992.

Uto, S., Computation of Incompressible Viscous Flow around a Marine Propeller, 2nd Report: Turbulent Flow Simulation, *Jpn. Soc. Nav. Archit. Ocean Eng.*, vol. **173**, pp. 67–75, 1993.

Xiao, W. and Walters, K., Computational Analysis of Marine Propeller Performance Using Transition-Sensitive Turbulence Modelling, *J. Fluids Eng.*, vol. **134**, 2012.

APPENDIX A. COMPUTATIONAL RESOURCES

Hardware

HP 650W 80
Red Hat Linux WS 4, 32/64 bit OS
Intel Xeon
HP 8GB (4x2GB) DDR2-667
HP 250GB SATA, HDD

Software

STARCCM+ 12.06